An embedding method for interface electronic structure calculations

1989 J. Phys.: Condens. Matter 1 599

(http://iopscience.iop.org/0953-8984/1/3/011)

J. Phys.: Condens. Matter 1 (1989) 599–610. Printed in the UK

An embedding method for interface electronic structure calculations

C P Farquhar† and J E Inglesfield‡
† Department of Physics, University of Edinburgh, Mayfield Road, Edinburgh EH9 3JZ, UK
‡ Daresbury Laboratory (Science and Engineering Research Council), Daresbury, Warrington WA4 4AD, UK

Received 13 July 1988

Abstract. A new method of determining interface electronic structure is described. Only a few layers on either side of the interface need to be explicitly considered. Each substrate is included via an embedding potential derived from the bulk Green function, which is added to the interface Hamiltonian. The technique allows localised interface states as well as the continuum of bulk states to be studied. Results are presented for the Al–Ni(001) interface, found self-consistently using the linearised augmented plane wave method.

1. Introduction

The changes in electronic structure which occur at the interface between two bulk media are important for determining the properties of electronic devices and point contacts and, more recently, for understanding semiconductor or metallic superlattices. Nearly perfect interfaces can be grown using techniques such as molecular beam epitaxy or chemical vapour deposition. Owing to the technological importance of these interfaces, it is useful to calculate their electronic properties from first principles, in order to give insight into their physical properties. The electronic structure of a superlattice can be calculated directly using ordinary band-structure techniques (Bylander and Kleinman 1987), although computational restraints limit the length of unit cell which can be treated. Here we are interested in the properties of a single interface, which can only be treated with conventional band-structure methods by using a relatively long unit cell, in order to reduce the interactions between neighbouring interfaces. This paper presents a new method of determining interface electronic structure, in which the effect of the substrates is included via embedding potentials added to the Hamiltonian in the interface region. The results of including these embedding potentials is to ensure that the interface wavefunction matches correctly the substrate wavefunctions. Using the embedding potential method, only one or two layers on either side of the interface need to be considered explicitly. Moreover, this new method reproduces the correct spectrum of states, both for the continuum of bulk states and for localised interface states.

This embedding method was introduced by Inglesfield (1981) and applied to surface electronic structure by Benesh and Inglesfield (1984), and in this paper it is generalised to the case of an interface between two bulk media. We also describe the details of the

0953-8984/89/030599 + 12 $02.50

interface calculation in which we use the linearised augmented plane-wave (LAPW) basis set in the interface region. The full potential is used in the interface region including warping terms, and its construction in the self-consistency cycle is described. Finally, we shall apply the technique to the Al–Ni(001) interface. Densities of states at fixed wavevector parallel to the interface, and charge densities are presented. Perhaps the most significant result is our observation of localised states in the Ni, which decay into the Al band gap.

2. Interface embedding

The basic principle of the embedding method is to consider explicitly only the finite region around the interface in which the potential differs significantly from the bulk, with each substrate being included in the Hamiltonian via an embedding potential term. Initially we derive a variational principle for the whole system (figure 1) in terms of an arbitrary trial wavefunction Φ, defined explicitly in the interface (region 3), but in the two substrates (regions 1 and 2) we take the trial wavefunction to be exact solutions of the Schrödinger equation at some energy ε, namely Ψ_1 and Ψ_2 in the respective regions 1 and 2. Ψ_1 and Ψ_2 match in amplitude Φ over S_1 and S_2, respectively. Note that the first derivative with respect to z of the total trial wavefunction is in general discontinuous across S_1 and S_2. The expectation value of the energy is given by

$$E = \langle\Psi|H|\Psi\rangle/\langle\Psi|\Psi\rangle \tag{1}$$

where Ψ is the total trial wavefunction, and $H = -\frac{1}{2}\nabla^2 + V(\boldsymbol{r})$. Hence

$$E = \left(\int_3 \Phi^* H\Phi \, \mathrm{d}^3\boldsymbol{r} + \varepsilon \int_1 \Psi_1^* \Psi_1 \, \mathrm{d}^3\boldsymbol{r} + \varepsilon \int_2 \Psi_2^* \Psi_2 \, \mathrm{d}^3\boldsymbol{r} - \tfrac{1}{2}(I_1 + I_2)\right) \times \left(\int_3 \Phi^*\Phi \, \mathrm{d}^3\boldsymbol{r} + \int_1 \Psi_1^* \Psi_1 \, \mathrm{d}^3\boldsymbol{r} + \int_2 \Psi_2^* \Psi_2 \, \mathrm{d}^3\boldsymbol{r}\right)^{-1} \tag{2}$$

where

$$I_1 = \int_{S_1} \left(\Phi^* \frac{\partial \Psi_1}{\partial z} - \Phi^* \frac{\partial \Phi}{\partial z}\right) \mathrm{d}^2\boldsymbol{r}_{S_1} \tag{3}$$

and

$$I_2 = \int_{S_2} \left(\Phi^* \frac{\partial \Phi}{\partial z} - \Phi^* \frac{\partial \Psi_2}{\partial z}\right) \mathrm{d}^2\boldsymbol{r}_{S_2}. \tag{4}$$

The fourth and fifth terms in (2) arise owing to the discontinuity in gradient of the wavefunction at S_1 and S_2. Note the sign change in the fifth term, to account for the opposite direction of $\boldsymbol{n}_2$ to $\boldsymbol{n}_1$.

We require a relationship between the solutions of the Schrödinger equation in the three regions. The results for substrate 1 will be derived, those for substrate 2 following in a similar manner. Writing $G_1^0(\boldsymbol{r}, \boldsymbol{r}')$ as the Green function in substrate 1, which has zero normal derivative on S_1, and using Green's theorem, gives (Inglesfield 1981)

$$\Psi_1(\boldsymbol{r}) = -\tfrac{1}{2} \int_{S_1} G_1^0(\boldsymbol{r}, \boldsymbol{r}_{S_1}) \frac{\partial \Psi_1(\boldsymbol{r}_{S_1})}{\partial n_1} \mathrm{d}^2\boldsymbol{r}_{S_1}. \tag{5}$$

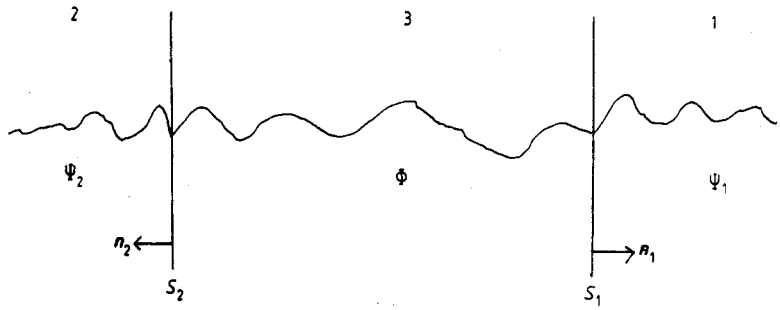

Figure 1. Interface region 3 is embedded onto substrate regions 1 and 2.

Inverting (5) leads to

$$\frac{\partial \Psi_1(\boldsymbol{r}_{S_1})}{\partial n_1} = -2 \int_{S_1} [G_1^0(\boldsymbol{r}_{S_1}, \boldsymbol{r}'_{S_1})]^{-1} \Phi(\boldsymbol{r}'_{S_1})\, \mathrm{d}^2 \boldsymbol{r}'_{S_1} \tag{6}$$

where we have used the property that $\Phi = \Psi_1$ on S_1.

The normalisation of Ψ_1 in region 1 is required. This is readily shown to be (Inglesfield 1981)

$$\int_1 |\Psi_1|^2 \, \mathrm{d}^3 \boldsymbol{r} = -\int_{S_1} \mathrm{d}^2 \boldsymbol{r}_{S_1} \int_{S_1} \mathrm{d}^2 \boldsymbol{r}'_{S_1}\, \Psi_1(\boldsymbol{r}_{S_1}) \frac{\partial [G_1^0(\boldsymbol{r}_{S_1}, \boldsymbol{r}'_{S_1})]^{-1}}{\partial E} \Psi_1(\boldsymbol{r}'_{S_1}). \tag{7}$$

The results for the other substrate (region 2) are identical, except that the normal derivative of Ψ_2 is in the direction of $\boldsymbol{n}_2$. Using (6) and (7) and their equivalents for region 2 gives

$$E = \left[\int_3 \Phi^* H \Phi \, \mathrm{d}^3 \boldsymbol{r} + I'_1 + I'_2 + \tfrac{1}{2} \left(\int_{S_1} \Phi^* \frac{\partial \Phi}{\partial z} \mathrm{d}^2 \boldsymbol{r}_{S_1} - \int_{S_2} \Phi^* \frac{\partial \Phi}{\partial z} \mathrm{d}^2 \boldsymbol{r}_{S_2} \right) \right] \times \left(\int_3 |\Phi|^2 \, \mathrm{d}^3 \boldsymbol{r} - I''_1 - I''_2 \right)^{-1} \tag{8}$$

where

$$I'_1 = \int_{S_1} \mathrm{d}^2 \boldsymbol{r}_{S_1} \int_{S_1} \mathrm{d}^2 \boldsymbol{r}'_{S_1}\, \Phi^*(\boldsymbol{r}_{S_1}) \left((G_1^0)^{-1} - \varepsilon \frac{\partial (G_1^0)^{-1}}{\partial E} \right) \Phi(\boldsymbol{r}'_{S_1}) \tag{9}$$

and

$$I''_1 = \int_{S_1} \mathrm{d}^2 \boldsymbol{r}_{S_1} \int_{S_1} \mathrm{d}^2 \boldsymbol{r}'_{S_1} \frac{\partial (G_1^0)^{-1}}{\partial E} \Phi(\boldsymbol{r}'_{S_1}) \tag{10}$$

with similar results for I'_2 and I''_2.

The energy is now given in terms of Φ, the trial wavefunction in the interface. We derive a Schrödinger equation from (8) by minimising the total energy with respect to

small changes in Φ. This leads to

$$\left(H + \tfrac{1}{2}\delta(\boldsymbol{r} - \boldsymbol{r}_{S_1})\frac{\partial}{\partial z} - \tfrac{1}{2}\delta(\boldsymbol{r} - \boldsymbol{r}_{S_2})\frac{\partial}{\partial z}\right)\Phi(\boldsymbol{r})$$
$$+ \delta(\boldsymbol{r} - \boldsymbol{r}_{S_1})\left[\int_{S_1} \mathrm{d}^2\boldsymbol{r}'_{S_1}\left((G_1^0)^{-1}(\boldsymbol{r}_{S_1}, \boldsymbol{r}'_{S_1}, \varepsilon)\right.\right.$$
$$\left.\left. + (E - \varepsilon)\frac{\partial (G_1^0)^{-1}(\boldsymbol{r}_{S_1}, \boldsymbol{r}'_{S_1}, \varepsilon)}{\partial E}\right|_{E=\varepsilon}\right)\Phi(\boldsymbol{r}'_{S_1})\Bigg]$$
$$+ \delta(\boldsymbol{r} - \boldsymbol{r}_{S_2})\left[\int_{S_2} \mathrm{d}^2\boldsymbol{r}'_{S_2}\left((G_2^0)^{-1}(\boldsymbol{r}_{S_2}, \boldsymbol{r}'_{S_2}, \varepsilon)\right.\right.$$
$$\left.\left. + (E - \varepsilon)\frac{\partial (G_2^0)^{-1}(\boldsymbol{r}_{S_2}, \boldsymbol{r}'_{S_2}, \varepsilon)}{\partial E}\right|_{E=\varepsilon}\right)\Phi(\boldsymbol{r}'_{S_2})\Bigg] = E\Phi(\boldsymbol{r}). \tag{11}$$

The wavefunction Φ given by this Schrödinger equation is a solution of the Hamiltonian in the interface region, and has the correct logarithmic derivatives on S_1 and S_2. The energy derivative terms correct the embedding potentials, so that to first order they are applicable to the energy E.

We choose to calculate the Green function in the interface region, rather than the individual wavefunctions, as we are interested in the continuum of bulk states, as well as localised states. This Green function is calculated at the same energies as the substrate embedding potentials; so $E = \varepsilon$ in (11). Also, expanding the interface Green function in terms of some basis $\{\varphi_i\}$, as

$$G(\boldsymbol{r}, \boldsymbol{r}') = \sum_{i,j} G_{ij}\varphi_i(\boldsymbol{r})\varphi_j^*(\boldsymbol{r}') \tag{12}$$

gives

$$\sum_{i,j} G_{ij}(H_{ki} - ES_{ki})\delta_{jl} = \delta_{kl} \tag{13}$$

where

$$H_{ki} = \int_1 \varphi_k^*(\boldsymbol{r})[-\tfrac{1}{2}\nabla^2 + V(\boldsymbol{r})]\varphi_i(\boldsymbol{r})\,\mathrm{d}^3\boldsymbol{r}$$
$$+ \tfrac{1}{2}\int_{S_1} \varphi_k^*(\boldsymbol{r}_{S_1})\frac{\partial}{\partial z}[\varphi_i(\boldsymbol{r}_{S_1})] - \tfrac{1}{2}\int_{S_2} \varphi_k^*(\boldsymbol{r}_{S_2})\frac{\partial}{\partial z}[\varphi_i(\boldsymbol{r}_{S_2})]$$
$$+ \int_{S_1} \mathrm{d}^2\boldsymbol{r}_{S_1}\int_{S_1} \mathrm{d}^2\boldsymbol{r}'_{S_1}\,\varphi_k^*(\boldsymbol{r}_{S_1})(G_1^0)^{-1}(\boldsymbol{r}_{S_1}, \boldsymbol{r}'_{S_1})\varphi_i(\boldsymbol{r}'_{S_1})$$
$$+ \int_{S_2} \mathrm{d}^2\boldsymbol{r}_{S_2}\int_{S_2} \mathrm{d}^2\boldsymbol{r}'_{S_2}\,\varphi_k^*(\boldsymbol{r}_{S_2})(G_2^0)^{-1}(\boldsymbol{r}_{S_2}, \boldsymbol{r}'_{S_2})\varphi_i(\boldsymbol{r}'_{S_2}) \tag{14}$$

and

$$S_{ki} = \int_3 \varphi_k^*(\boldsymbol{r})\varphi_i(\boldsymbol{r})\,\mathrm{d}^3\boldsymbol{r}. \tag{15}$$

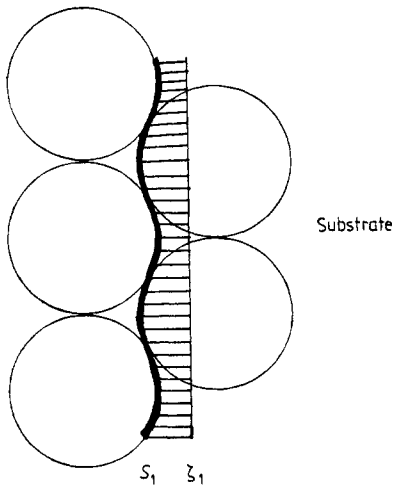

Figure 2. Illustration of the actual embedding surface S_1 and the shifted embedding surface ζ_1.

So

$$G_{ij} = (\mathbf{H} - E\mathbf{S})^{-1}_{ij}. \tag{16}$$

If the interface has two-dimensional periodicity, the problem can be reduced to the solution of the Schrödinger equation in one unit cell of this lattice, allowing us to define a Bloch embedding potential as

$$(G^0_{\boldsymbol{K}})^{-1} = \sum_j (G^0)^{-1}(\boldsymbol{r}, \boldsymbol{r}' - \boldsymbol{R}_j) \exp(-\mathrm{i}\boldsymbol{K} \cdot \boldsymbol{R}_j) \tag{17}$$

where the $\{\boldsymbol{R}_j\}$ are the two-dimensional direct lattice vectors.

From figure 2 we see that S_1 and S_2 are not flat surfaces, which is inconvenient as it means that the integrals in (14) are evaluated over awkwardly shaped regions. However, as described by Inglesfield (1981), the embedding potentials can be calculated over the shifted embedding surfaces ζ_1 and ζ_2, provided that a constant potential is included between the actual and shifted embedding surfaces. The embedding potentials are

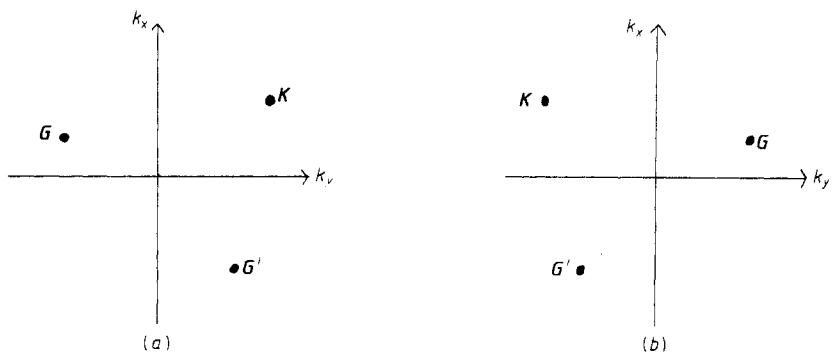

Figure 3. Wavevector and reciprocal-lattice vectors for $(G^0_{\boldsymbol{K}})^{-1}$ at (*a*) ζ_1 and (*b*) ζ_2.

chosen over ζ_1 and ζ_2 to give logarithmic derivatives on these surfaces which, when the Schrödinger equation is integrated through the constant potential in the shaded region in figure 2, produce the required logarithmic derivatives on S_1 and S_2. In future the embedding potentials will refer to those which are calculated over ζ_1 and ζ_2, respectively. These embedding potentials are conveniently calculated from the reflection properties of the bulk substrates (Benesh and Inglesfield 1984) and are given by

$$(G^0)^{-1} = \boldsymbol{\gamma}(\mathbf{I} - \mathbf{R})/2(\mathbf{I} + \mathbf{R}) \tag{18}$$

where $\boldsymbol{\gamma}$ is the matrix of wavevectors of scattered waves and $\mathbf{R}$ is the reflection matrix of the relevant substrate.

The embedding potential for a given material appropriate to a substrate on the right can be used on the left with no changes, assuming certain symmetry restrictions. To see this, consider the embedding potential $(G^0_{\boldsymbol{K}})^{-1}$ at some two-dimensional wavevector $\boldsymbol{K} = (K_x, K_y)$, expanded in terms of a set of reciprocal lattice vectors $\{\boldsymbol{G} = (G_x, G_y)\}$ at the right substrate. Figure 3(*a*) shows the geometry for two reciprocal lattice vectors $\boldsymbol{G}$ and $\boldsymbol{G}'$, looking onto the right embedding surface, with a set of axes x–y defined in the interface slab. Now, looking onto the left embedding surface, it is clear that we must evaluate $(G^0)^{-1}$ at $(K_x, -K_y)$ in terms of $\{(G_x, -G_y)\}$ as in figure 3(*b*). Now $(G^0)^{-1}$ for $(K_x, -K_y)$ expanded in $\{(G_x, -G_y)\}$ is the same as $(G^0)^{-1}$ for (K_x, K_y) expanded in $\{(G_x, G_y)\}$ if there is a mirror plane perpendicular to $\langle 0, 1\rangle$. Thus we can use the embedding potentials as calculated for ζ_1, at ζ_2 with no change, as long as the lattice has the required mirror plane. Lattices not having this symmetry could obviously be handled by modifying the construction of the embedding potentials.

3. Method of solution

Firstly, the geometry involved in the interface region is shown in figure 4. The interface is of width D. ζ_1 and ζ_2 are the embedding planes, which are usually taken to lie halfway between the layers of atoms in the bulk substrate, thus ensuring charge neutrality in the interface slab, which is important when constructing the new electrostatic potential in the self-consistent process. The basis to be used in the wavefunction expansion is defined over $-\tilde{D}/2$ to $+\tilde{D}/2$, in order that the wavefunction has sufficient variational freedom over the surfaces ζ_1 and ζ_2, to assume the correct logarithmic derivatives.

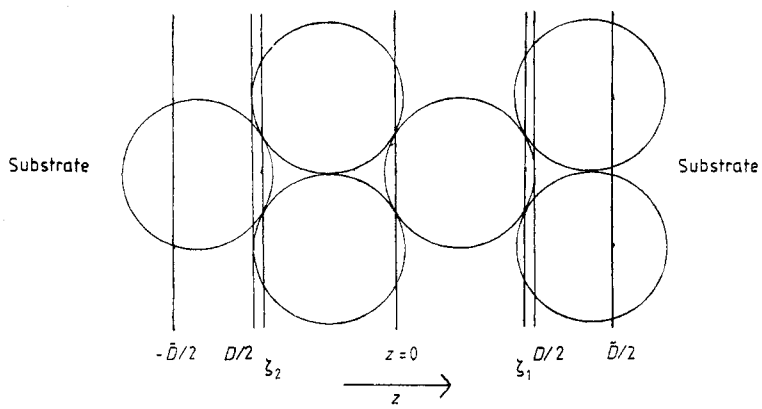

Figure 4. Geometry used in the interface.

The chosen basis set is the LAPW basis (Andersen 1975, Krakauer *et al* 1979), which is flexible and accurate. The LAPW basis is constructed around the simple muffin-tin form of potential, although the full potential is used to evaluate the matrix elements. In the interstitial region the LAPWs are defined to be

$$\varphi_{mn}(\boldsymbol{K}, \boldsymbol{r}) = \sqrt{\frac{2}{\Omega}} \exp(\mathrm{i}\boldsymbol{K}_m \cdot \boldsymbol{R}) \begin{cases} \cos(k_n z) \\ \sin(k_n z) \end{cases} \tag{19}$$

where

$$\boldsymbol{K}_m = \boldsymbol{K} + \boldsymbol{G}_m$$

$$k_n = n\pi/\tilde{D}$$

$$\Omega = AD.$$

$\boldsymbol{G}_m$ are the two-dimensional reciprocal-lattice vectors, and A is the area of the two-dimensional unit cell. The upper term in (19) is for n even, and the lower term for n odd. Inside the muffin-tin spheres, the scalar-relativistic equation is solved (Koelling and Harmon 1977), which is the Dirac equation with spin–orbit terms removed. The LAPW in each sphere α is taken to be a linear combination of the radial wavefunction $u_{l\alpha}$ and its energy derivative $\dot{u}_{l\alpha}$, multiplied by the spherical harmonics:

$$\varphi_{mn\alpha}(\boldsymbol{K}, \boldsymbol{r}) = \sum_{l,m} [A_{lm\alpha}(\boldsymbol{K}) u_{l\alpha}(\boldsymbol{r}) + B_{lm\alpha}(\boldsymbol{K}) \dot{u}_{l\alpha}(\boldsymbol{r})] Y_{lm}(\hat{\boldsymbol{r}}) \begin{cases} \mathrm{i}^l \\ \mathrm{i}^{l-1} \end{cases} \tag{20}$$

The $A_{lm\alpha}$ and $B_{lm\alpha}$ are chosen so that the LAPW is continuous in value and first derivative across the sphere boundary.

The actual potential in the interface includes non-spherical components inside the muffin tin potentials, which we expand in the form

$$V(\boldsymbol{r}) = \sum_{l,m \geqslant 0} [V^{\mathrm{c}}_{l,m}(r) \cos(m\varphi) + V^{\mathrm{s}}_{l,m}(r) \sin(m\varphi)] P_{l,m}(\theta). \tag{21}$$

In the interstitial region we have the 'warping' potential

$$V(\boldsymbol{r}) = \sum_{m,n} V_{mn} \exp(\mathrm{i}\boldsymbol{G}_m \cdot \boldsymbol{R}) \begin{cases} \cos(k_n z) \\ \sin(k_n z) \end{cases} + V_1 z + V_2 z^2$$

$$+ \sum_{m}{}' [V_{m+} \exp(+G_m z) + V_{m-} \exp(-G_m z)] \exp(\mathrm{i}\boldsymbol{G}_m \cdot \boldsymbol{R}). \tag{22}$$

The prime on the second sum excludes $m = 0$. This is the general solution of Poisson's equation, with the second, third and fourth terms being included owing to the absence of periodicity in the z direction.

The matrix elements between the LAPWs are similar to the surface case (Benesh and Inglesfield 1984, Inglesfield and Benesh 1988), although without the vacuum terms of course. Inside the muffin tins, they are identical. The interstitial elements are modified by the introduction of a second embedding plane ζ_2 instead of the surface–vacuum interface at $-D/2$, and there is also a second term arising from the embedding potential at ζ_2. The interstitial matrix elements of the warping potential are the most difficult to evaluate. Initially, all volume integrals are performed over the entire region from ζ_2 to

ζ_1, and over the whole of the muffin-tin spheres. However, in reality, the warping potential must only be included within the volume bounded by the true embedding surfaces S_1 and S_2 defined previously. Referring to figure 4, we see that the substrate and interface spheres may intersect the shifted embedding planes ζ_1 and ζ_2; so the previous volume integrals are modified by adding or subtracting the relevant muffin-tin cap integrals as appropriate, leaving us with the matrix elements of the warping potential between S_1 and S_2 as required (figures 1 and 2).

Once the matrix $\mathbf{H} - E\mathbf{S}$ is formed, it is inverted to obtain the interface Green function (equation (16)). From this, the local density of states is easily obtained via

$$\sigma(\boldsymbol{r}, E) = (1/\pi)\,\mathrm{Im}[G(\boldsymbol{r}, \boldsymbol{r}, E + \mathrm{i}\varepsilon)]. \tag{23}$$

The energy has a small imaginary part to shift it off the real axis, where the Green function has a branch cut. The density of states in a given region is obtained by integrating (23) over the required volume, and the charge density is obtained by integrating (23) over an energy range from below the valence bands to the Fermi energy, using contour integration. The core charge density, which is derived separately by solving the fully relativistic Dirac equation, is then added to the muffin-tin charge density, to form the total charge density in the muffin tins, expanded in the same form as the potential, given in equation (21). A plane-wave expansion is used for the charge density in the interstitial region.

The new potential for the second part of the self-consistent process is constructed in a similar manner to that described by Inglesfield and Benesh (1988) for the case of surfaces. To find the Hartree potential, the charge density is transformed to a new pseudo-charge density as described by Weinert (1981), which is the same as the actual charge density in the interstitial region and has the same multipole moments inside the muffin tins. Hence it gives rise to the same potential in the interstitial region, but it can be readily Fourier transformed, thus allowing the Fourier coefficients of the interstitial potential to be determined via Poisson's equation. After the interstitial potential has been evaluated, the construction of the potential inside the muffin tins becomes a boundary value problem.

When constructing the interstitial potential, it is necessary to include two boundary conditions, and these are taken to be the value of the potential at either side of the interface, which by definition are the same as in the bulk. Now, at an interface there is always a potential shift which is determined for metallic interfaces by the requirement that the Fermi level is constant across the interface in equilibrium. Knowing the position of the Fermi energy relative to the muffin-tin zero allows us to calculate the potential boundary conditions at the outset. For non-metallic junctions, we can either place the Fermi level at the centre of the band gap as a first approximation or use the experimentally measured potential shift if available. The coefficients of the interstitial potential (equation (22)) are adjusted using a least-squares fitting procedure to give the correct electrostatic shift. After the electrostatic potential has been constructed in this way, the exchange–correlation potential, evaluated in the local density approximation (Kohn and Sham 1965), is added. Once the new potential has been constructed, it is mixed with the input potential for that iteration, and the resulting potential is then used as the input potential for the next iteration. The alternating mixing factor scheme of Dederichs and Zeller (1983) is used once partial convergence has been achieved with a constant mixing factor, as we have found that the speed of convergence is considerably improved by using this method. This process is continued until the input and output potentials are in good agreement.

We have found that the method can give rise to instabilities in the charge density when using certain sizes of basis sets, either in the embedding potential expansion or in the number of LAPWs. The reason for this is as yet not fully understood, but we have encountered similar problems in surface calculations. At present, the problem is essentially avoided via trial and error.

4. Al–Ni(001) junction

As an example of the method, we apply it to the case of an ideal Al–Ni(001) interface to see how an s–p bonded metal joints onto a transition metal. The true lattice constants of Al and Ni, both of which have the face-centred cubic structure, are 7.600 au and 6.645 au, respectively. We use a lattice constant of 7.072 au for both materials, giving a square two-dimensional interface unit cell of side 5.000 au. One layer each of Al and Ni is considered in the interface region, using a basis set of 150 LAPWs, with three representative $\boldsymbol{K}$-points (Cunningham 1974) in the irreducible part of the two-dimensional Brillouin zone used to construct the charge density in the self-consistent cycle. After 30 iterations, we achieve convergence to within 0.004 Hartree within each muffin tin.

The density of states has been calculated at the points $\bar{\Gamma}(0.0, 0.0)$ and $\bar{X}(0.5, 0.0)$ of the two-dimensional Brillouin zone, which is related to the projected bulk face-centred cubic zone by a rotation of 45° about the k_z axis (figure 5). Referring first to the density of states at $\bar{\Gamma}$ in the Al muffin tin (figure 6(*a*)), we see an initial broad peak due to the Al s–p band and then a flat section from the overlap of the Ni s–p band inside the Al muffin tin. However, there is not much penetration of the Ni d bands into the Al muffin tins. Most interesting is the peak at 0.192 Hartree, which lies in the nearly free-electron gap of the bulk Al. The density of states in the Ni muffin tin (figure 6(*b*)) also shows the same peak, but it is not so evident owing to the proximity of the Ni d bands, which we have found to correlate well with the calculated bulk Ni band structure at $\bar{\Gamma}$. To investigate

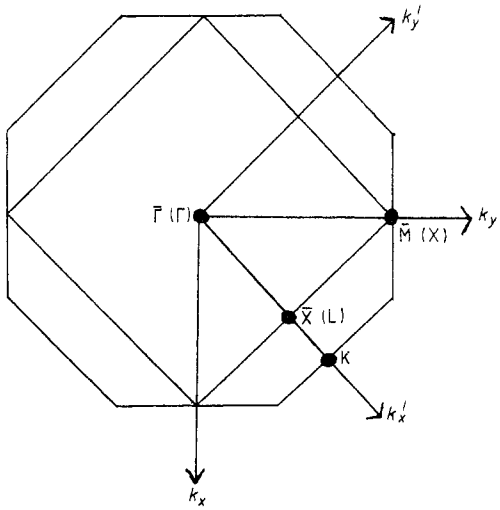

Figure 5. Relationship of two-dimensional Brillouin zone (k_x', k_y') to the projected bulk face-centred cubic zone (k_x, k_y).

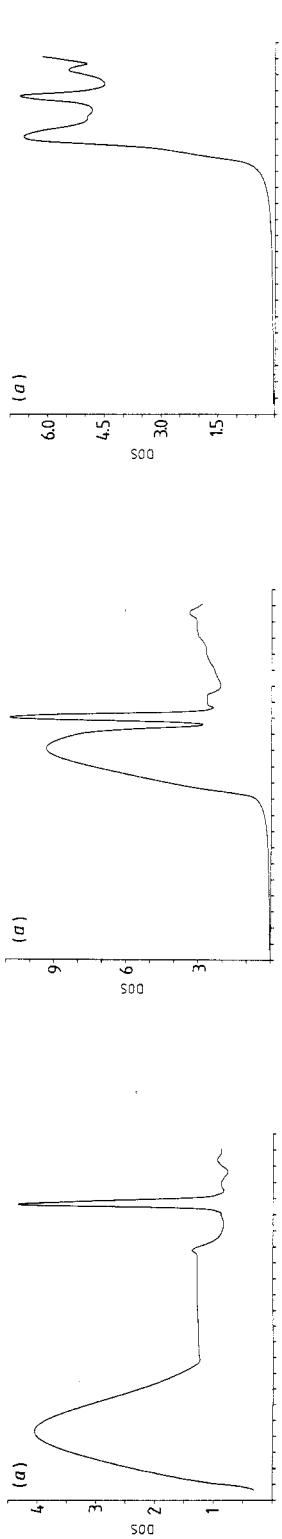

Figure 6. Density of states at $\bar{\Gamma}$ in (*a*) Al muffin tin and (*b*) Ni muffin tin. (*c*) Charge density of the interface state in the plane of Ni atoms.

Figure 7. Density of states at $\bar{X}$ in (*a*) Al muffin tin and (*b*) Ni muffin tin. (*c*) Charge density of the interface state in the plane of Ni atoms.

Figure 8. Density of states at $\bar{M}$ in (*a*) Al muffin and (*b*) Ni muffin tin. (*c*) Charge density of the interface state in the plane of Ni atoms.

this further, the charge density for this state has been plotted (figure 6(*c*)), which shows the localised state to be due to d_{z^2} orbitals on the Ni. It is therefore of Δ_1 symmetry, and in fact lies in a band gap of the bulk Ni Δ_1 bands, as well as in the Al gap, proving that it is not a bulk Ni state. It is a true interface state in the sense of decaying exponentially into both materials, but the fact that most of its charge density is localised on the Ni suggests that it is akin to a Ni surface state. The electronic structure of the Ni(001) surface shows d_{z^2} surface states at $\bar{\Gamma}$ near the top and bottom of the Δ_1 gap (Inglesfield and Benesh 1988), and these presumably become the interface state of our calculations. The Al is behaving almost like the vacuum as far as the Ni states are concerned, for energies in the Al band gap. Turning now to the density of states at $\bar{X}$ in the Al and Ni muffin tins (figures 7(*a*) and 7(*b*)) reveals a localised state of energy 0.12 Hartree on the Ni, which again lies in a bulk Al band gap. The charge density of the state (figure 7(*c*)) shows it to be due to either d_{zx} or d_{zy} orbitals on the Ni (the program symmetrises the charge density and so we cannot say which). Finally, the density of states at $\bar{M}$ (figures 8(*a*) and 8(*b*)) reveals a localised state at energy 0.216 Hartree, which is a d_{z^2} state on the Ni (figure 8(*c*)) of Z_1 symmetry. This state lies in a Z_1 symmetry gap in the Ni and below the Z_1 bands in Al (the states at this energy in Al are of Z_3 symmetry); so it cannot leak away into travelling waves in either substrate. The situation is therefore similar to before, with the state localised on the interface layer of Ni atoms decaying exponentially into the Al. Apart from these features, we find that the density of states is very similar to that in the respective bulk materials, indicating little interaction between the Al and Ni. This is in agreement with experimental data for this interface (Fargues *et al* 1985), which shows that there is only weak 3d–sp interaction and that the interface is indeed abrupt as we have assumed.

5. Conclusions

We have presented a new way of determining interface electronic structure, which can be readily added to any existing slab program. The benefits are obtained both in more physically realistic results and in computational efficiency when compared with the more usual slab superlattice techniques. The embedding potentials ensure that the calculated states are correctly broadened and allow interface states to be easily distinguished from the bulk band structure. At present, we are not able to calculate total energies at the interface, but this is planned for future work. Such calculations would be useful for comparison with experimetnal data on interface adhesion, such as that given by Martensson *et al* (1988).

Acknowledgments

CPF acknowledges financial support form the Carnegie Trust for the Universities of Scotland, and the Science and Engineering Research Council. This work was carried out on the FPS-164 attached processor at Daresbury Laboratory.

References

Andersen O K 1975 *Phys. Rev.* B **12** 3060–83

Benesh G A and Inglesfield J E 1984 *J. Phys. C: Solid State Phys.* **17** 1595–606
Bylander D M and Kleinman L 1987 *Phys. Rev.* B **36** 3229–36
Cunningham S L 1974 *Phys. Rev.* B **10** 4988–94
Dederichs P H and Zeller R 1983 *Phys. Rev.* B **28** 5462–72
Fargues D, Vergand F and Bonnelle C 1985 *Surf. Sci.* **163** 489–97
Inglesfield J E 1981 *J. Phys. C: Solid State Phys.* **14** 3795–806
Inglesfield J E and Benesh G A 1988 *Phys. Rev.* B **37** 6682–700
Koelling D D and Harmon B N 1977 *J. Phys. C: Solid State Phys.* **10** 3107–14
Kohn W and Sham L J 1965 *Phys. Rev.* **140** A1133–8
Krakauer H, Posternak M and Freeman A J 1979 *Phys. Rev.* B **19** 1706–19
Martensson N, Stenborg A, Björneholm O, Nilsson A and Andersen J N 1988 *Phys. Rev. Lett.* **60** 1731–4
Weinert M 1981 *J. Math. Phys.* **22** 2433–9